Computers and Mathematics with Applications 71 (2016) 1973–1989

Contents lists available at ScienceDirect

Computers and Mathematics with Applications

journal homepage: www.elsevier.com/locate/camwa

Mathematical modeling and analysis of the Delta robot with flexible links

Yong-Lin Kuo *

Graduate Institute of Automation and Control, National Taiwan University of Science and Technology, Taipei City, 10607, Taiwan

ARTICLE INFO

Article history:
Received 17 July 2015
Received in revised form 11 March 2016
Accepted 19 March 2016
Available online 11 April 2016

Keywords:
Delta robot
Flexible links
Kineto-elasto-dynamics

ABSTRACT

This paper presents a mathematically dynamic model of a Delta robot with flexible links. The mathematical models of the robot cannot be represented by partial differential equations, so this paper utilizes the kineto-elasto-dynamics and the finite element method to perform a mathematical model. Each link of the robot is modeled by multiple beam elements with an axial displacement, an axial torsion, and two transverse displacements. In literature, element assembling usually imposes a set of algebraic constraint equations, which are difficultly solved simultaneously. This paper proposes an alternative approach. A set of global variables based on the D–H method is defined, and the Euler–Lagrange's equation is applied to derive the model without using any constraint equations. The developed model is a set of linear time-varying differential equations, which can describe the flexible motions with respect to the rigid body configuration. Furthermore, the natural frequency analysis and the convergence analysis are performed first, and then two types of paths are designed for the motions of the end-effector. The first path is a constant-speed circular motion in order to demonstrate the numerical simulations of the model at the steady state, and the second path is an inverted-U path, which is commonly used to operate a pick-to-place motion in industry.

1. Introduction

Parallel manipulators exhibit high stiffness in nearly all configurations, and the manipulators can perform high-speed motions to complete specific tasks. One of the most famous spatial parallel manipulators is the Delta robot, which has three translational degrees of freedom [1–4]. In recent decades, many papers assuming its links as rigid bodies study its kinematic analysis [2,5–7] and dynamic modeling [8–12] to predict the kinematic and dynamic behaviors through the accurate mathematical formations. Since the manipulator is usually designed as a lightweight mechanism to operate a high-speed motion with high loads, it becomes more significant to have highly accurate predictions, especially for some applications such as laser cutting or machining. Thus, the flexibility of links, joints, or fixed/moving bases should be taken into account in the mathematical modeling.

Some researches consider flexible links in the manipulators. Book proposed a recursive Lagrangian dynamic modeling of flexible manipulator arms [13]. The kinematics of rotary joints and flexible links are described by 4×4 transformation matrices, and the link deflections are approximated by summations of assumed link shapes. Géradin and Cardona presented the flexible multibody dynamics [14]. A finite element approach is utilized to model flexible links, and kinematic joints are regarded as algebraic constraints. Thus, a flexible multibody system is represented by a set of differential–algebraic

* Tel.: +886 2 27303696; fax: +886 2 27301265.
E-mail address: kuo@mail.ntust.edu.tw.

http://dx.doi.org/10.1016/j.camwa.2016.03.018
0898-1221/

equations. For the modeling of flexible Delta robots, Fattah et al. studied the dynamics of the manipulator with flexible links [15]. The finite element method was applied to model the flexible links, and the Euler–Lagrange formulation was used to derive the equations of motion of the uncoupled links. Besides, the method of the natural orthogonal complement was used to eliminate the constraint forces and to derive the minimum number of equations of motion. Liu et al. also derived the manipulator with flexible links by the finite element method [16]. An element was modeled with eighteen degrees of freedom, which includes axial, torsional, and two bending motions. In addition, the kinematics and dynamic constraint equations were used in the finite element formulations. Rognant et al. presented a procedure for the elastodynamic modeling of industrial robots based on a 3-D space generalization of the equivalent rigid link system description, the finite element method, and the Lagrange principle [17]. Zhang et al. formulated a dynamic model by using the substructure displacement method and verified the model through the software ANSYS [18]. Březina et al. summarized important steps for the design of a Delta robot for a given application by using a model-based approach [19].

Cleghorn et al. presented a kineto-elasto-dynamics modeling for flexible mechanisms, where a translating and rotating beam model was proposed and implemented on flexible four-bar mechanism based on the finite element method [20]. The model incorporated a longitudinal load into the transverse deflection of beam, and this can provide more accurate vibration predictions. This approach is based on a prescribed rigid body motion, so it can affect a flexible motion. Besides, the authors developed a procedure for determining the steady-state solution of the flexible four-bar mechanism by truncated Fourier series [21]. After that, Piras et al. extended the procedure and applied it to a planar parallel manipulator with flexible links, where the links are allowed to have bending and tensional motions [22]. Gaultier et al. also extended the procedure and presented a spatial translating and rotating beam model, and the presented procedure was applied to a spatial flexible serial manipulator [23].

This paper first introduces the dynamic equations of a Delta robot with rigid links and then extends Cleghorn's approach to establish a kineto-elasto-dynamic modeling of a Delta robot with flexible links. Thus, a beam element undergoes a three-dimensional motion, and the flexible deflections of the beam element are considered with axially tensional, axially torsional and two-directional bending motions. To apply the finite element method, all beam elements should be assembled. In literature, a set of algebraic constraint equations based on the geometry of the manipulators is imposed to the finite element equations, and this leads to a set of differential–algebraic equations, which are complicated and difficult to be solved simultaneously. This paper presents an alternative approach without using any constraint equations. A set of global variables based on the D–H method is defined to describe the flexible motion of the manipulator. By using this set of global variables, all beam elements can be assembled, and then the result leads to a set of linear time-varying ordinary differential equations, which can be easily solved by most of numerical integrations. This paper is organized as follows. Section 2 introduces the kinematics and dynamics of the robot with rigid links. Section 3 presents the finite element modeling of the robot with flexible links. Section 4 defines a set of the global variables to assemble all beam elements. Section 5 demonstrates two kineto-elasto-dynamic simulations. The conclusions are summarized in Section 6.

2. Kinematics and dynamics of a Delta robot with rigid links

A Delta robot has a rigid moving platform, which is connected to a fixed base through three sets of kinematic chains (see Fig. 1). Each chain (A_iB_i and B_iD_i, where $i = 1, 2, 3$) consists of two rigid links that are connected at point B_i, which has two rotational degrees of freedom. There are three actuators fixed on points A_i of the base, and each actuator drives one link of the kinematic chain. Triangle $A_1A_2A_3$ is the fixed based, and a global coordinate system XYZ is defined based on point O. Triangle $D_1D_2D_3$ refers to the moving platform and is called the end-effector, where point P is a central point on the moving platform. Besides, point D_i has two rotational degrees of freedom, so the link B_iD_i ($i = 1, 2, 3$) is usually designed as a four-bar mechanism, or points B_i and D_i are placed by two spherical joints. If the robot is rigid, the end-effector has three translational degrees of freedom. This can be verified by the Grubler [24] or Kutzbach criterion [25] as

$$\text{DOF} = \lambda(n - j - 1) + \sum_i f_i \tag{1}$$

where DOF is the degree of freedom of a mechanism; λ is the degree of freedom of the space in which a mechanism is intended to function; n is the number of links in a mechanism which includes the fixed link; j is the number of joints in a mechanism, assuming that all the joints are binary; f_i is the degrees of relative motion permitted by joint i. By referring to Fig. 1, the mechanism is operated in a three-dimensional space, so λ equal to six due to three translational motions and three rotational motions. The mechanism consists of a fixed based, a moving platform, three upper links, and three lower links, so n equal to eight. Each kinematic chain has three joints, so j equal to nine. Point A_i has one rotational motion, point B_i has two rotational motions, and point D_i has two rotational motions, so the sum of f_i equal to fifteen. By substituting all values into Eq. (1), the DOF equal to three.

2.1. Denavit–Hartenberg transformation matrices

Denavit–Hartenberg (D–H) transformation matrices can be used to define the relationship between two coordinate systems. The matrices will be used to derive the kinematics of the robot. Define three rotation matrices and three translation

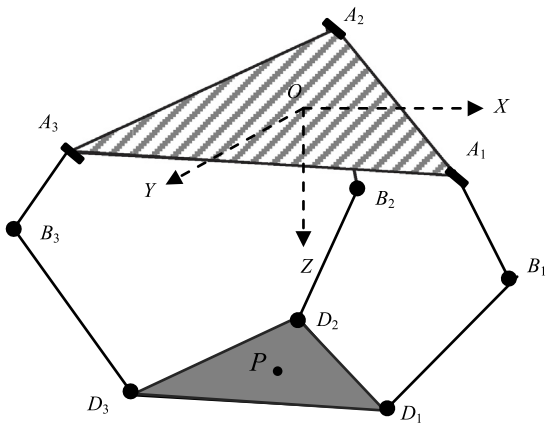

Fig. 1. The spatial parallel manipulator. (The upper and lower triangles refer to the fixed based and the end-effector, respectively.)

matrices as [26]

$$\mathbf{R}_x(\alpha) = \begin{bmatrix} 1 & 0 & 0 & 0 \\ 0 & c_\alpha & -s_\alpha & 0 \\ 0 & s_\alpha & c_\alpha & 0 \\ 0 & 0 & 0 & 1 \end{bmatrix}, \quad \mathbf{R}_y(\alpha) = \begin{bmatrix} c_\alpha & 0 & s_\alpha & 0 \\ 0 & 1 & 1 & 0 \\ -s_\alpha & 0 & c_\alpha & 0 \\ 0 & 0 & 0 & 1 \end{bmatrix}, \quad \mathbf{R}_z(\alpha) = \begin{bmatrix} c_\alpha & -s_\alpha & 0 & 0 \\ s_\alpha & c_\alpha & 0 & 0 \\ 0 & 0 & 1 & 0 \\ 0 & 0 & 0 & 1 \end{bmatrix}$$

$$\mathbf{T}_x(d) = \begin{bmatrix} 1 & 0 & 0 & d \\ 0 & 1 & 0 & 0 \\ 0 & 0 & 1 & 0 \\ 0 & 0 & 0 & 1 \end{bmatrix}, \quad \mathbf{T}_y(d) = \begin{bmatrix} 1 & 0 & 0 & 0 \\ 0 & 1 & 0 & d \\ 0 & 0 & 1 & 0 \\ 0 & 0 & 0 & 1 \end{bmatrix}, \quad \mathbf{T}_z(d) = \begin{bmatrix} 1 & 0 & 0 & 0 \\ 0 & 1 & 0 & 0 \\ 0 & 0 & 1 & d \\ 0 & 0 & 0 & 1 \end{bmatrix} \tag{2}$$

where α is a rotating angle between two coordinate systems; d is a translating displacement between two coordinate systems; c_α and s_α represent $\cos\alpha$ and $\sin\alpha$, respectively.

2.2. Kinematic formations of the manipulator

One assumes that the size of each kinematic chain is identical and is shown in Fig. 2, where L_1, L_2, r_A, and r_B represent the lengths of B_iD_i, A_iB_i, OA_i, and D_iP, respectively; ϕ_{1i} is the rotating angle of link A_iB_i, and ϕ_{2i} and ϕ_{3i} represent the rotating angles of link B_iD_i; the angle θ_i defines the positions of point A_i, because the distance from the origin to point A_i is expressed as r_A. To locate the position of point P by using the D–H transformation matrices, several coordinate systems $x_jy_jz_j$ ($j = 0, 1, 2, 3$) are defined (see Fig. 2), and then a sequence of matrix multiplications referring to coordinate transformations from the fixed reference frame to the end-effector frame is written as

$$\mathbf{R}_z(\theta_i)\mathbf{T}_x(r_A)\mathbf{R}_y(\phi_{1i})\mathbf{T}_x(L_1)\mathbf{R}_y(\phi_{2i})\mathbf{R}_z(\phi_{3i})\mathbf{T}_x(L_2)\mathbf{R}_z(-\phi_{3i})\mathbf{R}_y(-\phi_{i2})\mathbf{T}_x(-r_B) = \left[\begin{array}{c|c} \mathbf{R}_{3\times3} & \mathbf{P}_{3\times1} \\ \hline \mathbf{0}_{1\times3} & 1 \end{array}\right] \tag{3}$$

where $\mathbf{R}_{3\times3}$ and $\mathbf{P}_{3\times1}$ represent the attitude matrix and the position vector of point P, respectively. Expanding the sequence of matrices leads to the right-hand side of Eq. (3). Since the robot only provides three translating motions, matrix $\mathbf{R}_{3\times3}$ equal to an identity matrix, and the position vector can be written as

$$\boldsymbol{P}_{3\times1} = \begin{bmatrix} X_P \\ Y_P \\ Z_P \end{bmatrix} = \begin{bmatrix} \cos\theta_i(r_A - r_B + L_1\cos\phi_{1i} + L_2\cos(\phi_{1i} + \phi_{2i})\cos\phi_{3i}) - L_2\sin\theta_i\sin\phi_{3i} \\ \sin\theta_i(r_A - r_B + L_1\cos\phi_{1i} + L_2\cos(\phi_{1i} + \phi_{2i})\cos\phi_{3i}) + L_2\sin\theta_i\cos\phi_{3i} \\ L_1\sin\phi_{1i} + L_2\sin(\phi_{1i} + \phi_{2i})\cos\phi_{3i} \end{bmatrix} \tag{4}$$

with $i = 1, 2$ and 3. Vector $\boldsymbol{P}_{3\times1}$ represents the coordinates of point P with respect to the fixed reference frame XYZ.

In order to eliminate the passive joint angles ϕ_{2i} and ϕ_{3i}, Eq. (4) represents three equations. Each equation is squared, and then all squared equations are summed up as

$$(X_P - X_i)^2 + (Y_P - Y_i)^2 + (Z_P - Z_i)^2 = L_2^2 \tag{5}$$

where

$$X_i = (r + L_1\cos\phi_{1i})\cos\theta_i, \qquad Y_i = (r + L_1\cos\phi_{1i})\sin\theta_i, \qquad Z_i = -L_1\sin\phi_{1i}, \qquad r = r_A - r_B. \tag{6}$$

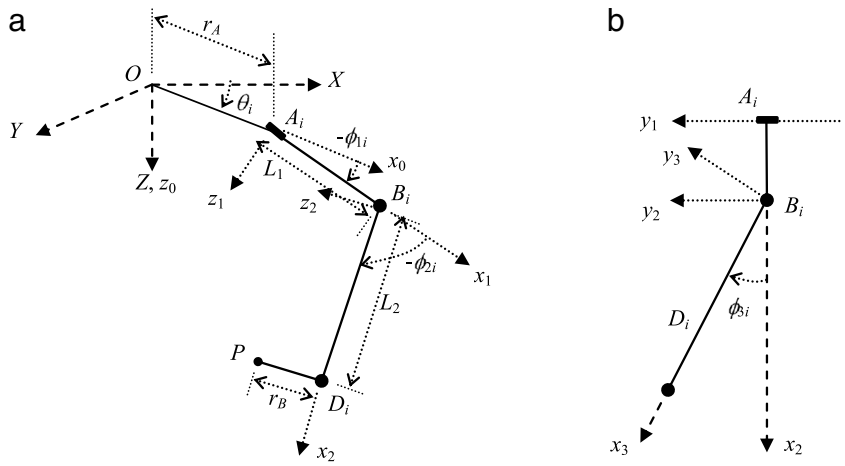

Fig. 2. A kinematic chain.

2.2.1. Direct kinematics of the manipulator

The direct kinematics determines the coordinates (X_P, Y_P, Z_P) of point P based on a set of given active joint angles ϕ_{1i}. Eq. (5) represents three spherical equations in terms of three given active joint angles. Thus, the coordinates are the intersection of the three spheres and can be obtained by simultaneously solving Eq. (5). In general, there are two possible solutions referring to two configurations [6].

2.2.2. Indirect kinematics of the manipulator

The indirect kinematics determines the active joint angles ϕ_{1i} based on a given coordinates (X_P, Y_P, Z_P), so Eq. (5) represents the equation for the ith kinematic chain. Thus, the active joint angles can be obtained by solving the equation, and Eq. (5) can be rewritten as

$$l_i \cos\phi_{1i} + m_i \sin\phi_{1i} = n_i \tag{7}$$

where

$$\begin{aligned} &l_i = 2rL_1 - 2L_1X_P\cos\theta_i - 2L_1Y_P\sin\theta_i, \qquad m_i = 2L_1Z_P, \\ &n_i = 2rX_P\cos\theta_i - 2rY_P\sin\theta_i + X_P^2 + Y_P^2 + Z_P^2 + L_1^2 - L_2^2 + r^2. \end{aligned} \tag{8}$$

There are four possible solutions. Please refer to Ref. [6] for more details.

2.3. Dynamic formations of the robot

The dynamic equations of the robot can be derived by the Euler–Lagrange's equations as

$$\frac{d}{dt}\left(\frac{\partial L_m}{\partial q}\right) - \frac{\partial L_m}{\partial q} = Q \tag{9}$$

where q refers to X_P, Y_P, Z_P, and ϕ_i $(i = 1, 2, 3)$; Q refers to the applied forces (F_{PX}, F_{PY} and F_{PZ}) at point P and the applied torques τ_i $(i = 1, 2, 3)$ to the active joints; L_m is the Lagrangian, which is obtained by the following equation as

$$L_m = T_m - V_m \tag{10}$$

in which T_m and V_m respectively refer to the kinetic energy and the potential energy as

$$T_m = \frac{1}{2}m_P(\dot{X}_P^2 + \dot{Y}_P^2 + \dot{Z}_P^2) + \frac{1}{6}m_1L_1^2\sum_i \dot{\phi}_{1i}^2 + \frac{1}{2}m_2\sum_i(\dot{X}_P^2 + \dot{Y}_P^2 + \dot{Z}_P^2 + L_1^2\dot{\phi}_{1i}^2) \tag{11}$$

$$V_m = m_PgZ_P + \frac{1}{2}m_1gL_1\sum_i \sin\phi_{1i} + m_2g\sum_i(Z_P + L_1\sin\phi_{1i}) \tag{12}$$

where m_P, m_1 and m_2 are the masses of the end-effector, the upper link and the lower link, respectively.

By substituting Eqs. (10)–(12) into (9), the equations of motion of the Delta robot can be written as

$$(m_P + 3m_2)\ddot{X}_P - 2\sum_i \lambda_i (X_P + r\cos\theta_i - L_1\cos\phi_{1i}\cos\theta_i) = F_{PX} \tag{13}$$

$$(m_P + 3m_2)\ddot{Y}_P - 2\sum_i \lambda_i (Y_P + r\sin\theta_i - L_1\cos\phi_{1i}\sin\theta_i) = F_{PY} \tag{14}$$

$$(m_P + 3m_2)\ddot{Z}_P - 2\sum_i \lambda_i (Z_P - L_1\sin\phi_{1i}) + (m_P + 3m_2)g = F_{PZ} \tag{15}$$

$$\left(\frac{1}{3}m_1 + m_2\right)L_1^2\ddot{\phi}_{1i} + \left(\frac{1}{2}m_1 + m_2\right)gL_1\cos\phi_{1i} - 2\lambda_i L_1[(X_P\cos\theta_i + Y_P\sin\theta_i + r)\sin\phi_{1i} - Z_P\cos\phi_{1i}] = \tau_i$$
$$(i = 1, 2, 3) \tag{16}$$

where λ_i are the Lagrange multipliers.

Since the rigid Delta robot has three degrees of freedom, the robot's configuration can be described by three variables, which are the positions (X_P, Y_P, Z_P) of the end-effector or the active joint angles ϕ_i $(i = 1, 2, 3)$. Thus, the two sets of variables are dependent, so it is necessary to impose constraint equations as shown in Eq. (5) so as to solve all variables. In other words, Eqs. (13)–(16) represent six dynamic equations in terms of nine variables X_P, Y_P, Z_P, ϕ_{1i}, and λ_i $(i = 1, 2, 3)$, so three constraint equations shown in Eq. (5) should be included and simultaneously solved for the nine variables. Thus, the nine equations are a set of differential–algebraic equations. For practical applications, the applied torques can be treated as command signals to accomplish the torque control of motors (while the motors are mounted on the active angles), and the command signals (the applied torques) can be determined by following the procedure as

1. By performing the path planning of the end-effector, its position (X_P, Y_P, Z_P) can be obtained.
2. By applying the inverse of kinematics, the active joint angles ϕ_{1i} $(i = 1, 2, 3)$ can be determined. Also, the passive joint angles ϕ_{2i}, and ϕ_{3i} $(i = 1, 2, 3)$ can be obtained.
3. By differentiating Eq. (5), the time derivatives of the variables X_P, Y_P, Z_P, ϕ_{1i}, ϕ_{2i}, and ϕ_{3i} $(i = 1, 2, 3)$ can be obtained.
4. By substituting X_P, Y_P, Z_P, ϕ_{1i}, ϕ_{2i}, and ϕ_{3i} $(i = 1, 2, 3)$ as well as their time derivatives into Eqs. (13)–(15), the Lagrange multipliers λ_i $(i = 1, 2, 3)$ can be obtained, where the applied forces are treated as given quantities.
5. By using Eq. (16), the applied torques τ_i $(i = 1, 2, 3)$ can be determined.

Therefore, by applying the above procedure, Eqs. (13)–(16) can be used for a real-time control of the Delta robot.

3. Finite element formulations of a Delta robot with flexible links

One assumes that the flexible motion of the robot is considered to be far smaller than the rigid body motion, so the flexible motion does not affect the rigid body motion. Before performing further formulations, the kinematics of the robot should be evaluated, and each link is discretized as multiple beam elements. This section starts from the modeling of a beam element. To assemble all beam elements, one defines a set of global variables to describe the flexible motion of the robot and determines the relationship between them and the nodal variables of each beam element. If the relationship is well defined, the global finite element equations can be obtained. Next section will present how to relate the nodal variables and the global variables for each beam element.

The modeling of the robot is based on the finite element method, and a floating frame [27] is used to establish the model. To formulate the finite element equations of the robot, one models a spatial translating and rotating beam element (see Fig. 3), which is subjected to an axial deformation, a torsional deformation, and two bending deformations. These deformations perform three displacements and one torsional angle. The modeling of these elastic deformations is based on the Euler–Bernoulli beam theory. Based on the finite element method, the deformations are approximated as

$$u(x, t) = \boldsymbol{N}_u^T(x)\boldsymbol{\delta}_e(t), \qquad v(x, t) = \boldsymbol{N}_v^T(x)\boldsymbol{\delta}_e(t), \qquad w(x, t) = \boldsymbol{N}_w^T(x)\boldsymbol{\delta}_e(t), \qquad \varphi(x, t) = \boldsymbol{N}_\varphi^T(x)\boldsymbol{\delta}_e(t) \tag{17}$$

where u, v and w are the elastic displacement of the arbitrary point on the x-, y- and z-axes, respectively; φ is the torsional angle on the x-axis; $\boldsymbol{N}_u, \boldsymbol{N}_v, \boldsymbol{N}_w$ and $\boldsymbol{N}_\varphi$ are the column vectors of the shape functions related to the three elastic displacements and the torsional angle; $\boldsymbol{\delta}_e$ is a column vector in terms of the nodal variables of the beam element.

Referring to Fig. 3, a coordinate system is defined at the left-end point, and then the absolute velocity of an arbitrary point on the beam element is expressed as

$$\boldsymbol{V}_e(x, t) = \boldsymbol{V}_o(t) + \boldsymbol{\omega}_o \times \boldsymbol{r}_e(x, t) + \dot{\boldsymbol{r}}_e(x, t) = \begin{bmatrix} V_{ox} + \omega_{oy}w(x, t) - \omega_{oz}v(x, t) + \dot{u}(x, t) \\ V_{oy} - \omega_{ox}w(x, t) + \omega_{oz}(x + u(x, t)) + \dot{v}(x, t) \\ V_{oz} + \omega_{ox}v(x, t) - \omega_{oy}(x + u(x, t)) + \dot{w}(x, t) \end{bmatrix} \tag{18}$$

where $\boldsymbol{V}_o = [V_{ox} \quad V_{oy} \quad V_{oz}]^T$ is the velocity at the left-end point of the beam element (see Fig. 3), $\boldsymbol{\omega}_o = [\omega_{ox} \quad \omega_{oy} \quad \omega_{oz}]^T$ is the angular velocity of the beam element (see Fig. 3), and $\boldsymbol{r}_e = [x + u(x, t) \quad v(x, t) \quad w(x, t)]^T$ is the position vector of the arbitrary point on the beam element. Based on the kinematics of the robot, $\mathbf{V}_o$ can be obtained by differentiating the positions at the left-end points for all beam elements, and $\boldsymbol{\omega}_o$ can be obtained by performing the coordinate transformations regarding to the angular velocities of the active and passive angles ϕ_{1i}, ϕ_{2i}, and ϕ_{3i} $(i = 1, 2, 3)$.

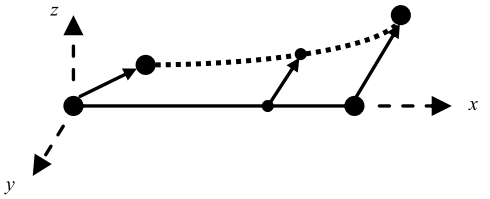

Fig. 3. A spatial beam element.

3.1. Kinetic energy of the beam element

One assumes that the beam element has a uniform density and a constant cross-sectional area. The kinetic energy of the beam element is given as

$$T_e = \frac{1}{2}\rho A \int_0^l \boldsymbol{V}_e^2 dx + \frac{1}{2}\rho I_1 \int_0^l (\omega_{ox} + \dot{\varphi})^2 dx \tag{19}$$

where ρ is the mass density, A is the cross-sectional area, l is the length of the beam element, I_1 is the moment of area along the x-axis.

Substituting Eqs. (17) and (18) into (19) leads to

$$T_e = \frac{1}{2}\dot{\boldsymbol{\varphi}}_e^T \mathbf{M}_e \dot{\boldsymbol{\varphi}}_e + \dot{\boldsymbol{\varphi}}_e^T \mathbf{B}_e \boldsymbol{\varphi}_e + \frac{1}{2}\boldsymbol{\varphi}_e^T \mathbf{M}_s \boldsymbol{\varphi}_e + \boldsymbol{Y}_e^T \boldsymbol{\varphi}_e + \boldsymbol{Z}_e^T \dot{\boldsymbol{\varphi}}_e + C_e \tag{20}$$

where

$$\mathbf{M}_e = \rho A \int_0^l (\boldsymbol{N}_u \boldsymbol{N}_u^T + \boldsymbol{N}_v \boldsymbol{N}_v^T + \boldsymbol{N}_w \boldsymbol{N}_w^T) dx + \rho I_x \int_0^l \boldsymbol{N}_\varphi \boldsymbol{N}_\varphi^T dx \tag{21}$$

$$\begin{aligned}\mathbf{M}_s = {} & \rho A \int_0^l [(\omega_{oy}^2 + \omega_{oz}^2)\boldsymbol{N}_u \boldsymbol{N}_u^T + (\omega_{ox}^2 + \omega_{oz}^2)\boldsymbol{N}_v \boldsymbol{N}_v^T + (\omega_{ox}^2 + \omega_{oy}^2)\boldsymbol{N}_w \boldsymbol{N}_w^T \\ & - \omega_{ox}\omega_{oy}(\boldsymbol{N}_u \boldsymbol{N}_v^T + \boldsymbol{N}_v \boldsymbol{N}_u^T) - \omega_{ox}\omega_{oz}(\boldsymbol{N}_u \boldsymbol{N}_w^T + \boldsymbol{N}_w \boldsymbol{N}_u^T) - \omega_{oy}\omega_{oz}(\boldsymbol{N}_v \boldsymbol{N}_w^T + \boldsymbol{N}_w \boldsymbol{N}_v^T)] dx\end{aligned} \tag{22}$$

$$\mathbf{B}_e = \rho A \int_0^l [\omega_{oz}(\boldsymbol{N}_u \boldsymbol{N}_v^T - \boldsymbol{N}_v \boldsymbol{N}_u^T) + \omega_{oy}(\boldsymbol{N}_w \boldsymbol{N}_u^T - \boldsymbol{N}_u \boldsymbol{N}_w^T) + \omega_{ox}(\boldsymbol{N}_v \boldsymbol{N}_w^T - \boldsymbol{N}_w \boldsymbol{N}_v^T)] dx \tag{23}$$

$$\begin{aligned}\boldsymbol{Y}_e = {} & \rho A \int_0^l [(\omega_{oz} V_{oy} - \omega_{oy} V_{oz} + (\omega_{oy}^2 + \omega_{oz}^2)x) N_v + (\omega_{ox} V_{oz} - \omega_{oz} V_{ox} + \omega_{ox}\omega_{oy} x)\boldsymbol{N}_v \\ & + (\omega_{oy} V_{ox} - \omega_{ox} V_{oy} + \omega_{ox}\omega_{oz} x)\boldsymbol{N}_w] dx\end{aligned} \tag{24}$$

$$\boldsymbol{Z}_e = \rho A \int_0^l [V_{ox}\boldsymbol{N}_u + (V_{oy} + \omega_{oz} x)\boldsymbol{N}_v + (V_{oz} - \omega_{oy} x)\boldsymbol{N}_w dx] + \rho I_x \int_0^l \omega_{ox} \boldsymbol{N}_\varphi dx \tag{25}$$

$$C_e = \frac{1}{2}\rho A l \left[V_{ox}^2 + V_{oy}^2 + V_{oz}^2 + \frac{1}{3}(\omega_{oy}^2 + \omega_{oz}^2) l^2 + (V_{oy}\omega_{oz} - V_{oz}\omega_{oy}) l \right] + \frac{1}{2}\rho I_x l \omega_{ox}^2. \tag{26}$$

3.2. Strain energy of the beam element

The beam element is considered with axial, lateral and torsional strains. Thus, the strain energy is given as

$$V_e = \frac{1}{2}EA \int_0^l \left(\frac{\partial u}{\partial x}\right)^2 dx + \frac{1}{2}EI_z \int_0^l \left(\frac{\partial^2 v}{\partial x^2}\right)^2 dx + \frac{1}{2}EI_y \int_0^l \left(\frac{\partial^2 w}{\partial x^2}\right)^2 dx + \frac{1}{2}GI_x \int_0^l \left(\frac{\partial \varphi}{\partial x}\right)^2 dx \tag{27}$$

where E and G are the elastic and shear moduli; I_x, I_y and I_z are the moments of area with respect to x-, y- and z-axes, respectively.

Substituting Eqs. (17) and (18) into (27) leads to

$$V_e = \frac{1}{2}\boldsymbol{\delta}_e^T \mathbf{K}_e \boldsymbol{\delta}_e \tag{28}$$

where

$$\mathbf{K}_e = EA \int_0^l \boldsymbol{N}_{ux} \boldsymbol{N}_{ux}^T dx + EI_z \int_0^l \boldsymbol{N}_{vxx} \boldsymbol{N}_{vxx}^T dx + EI_y \int_0^l \boldsymbol{N}_{wxx} \boldsymbol{N}_{wxx}^T dx + GI_x \int_0^l \boldsymbol{N}_{\varphi x} \boldsymbol{N}_{\varphi x}^T dx \tag{29}$$

where the subscripts x and xx represent the first and second partial derivatives.

3.3. Gravitational potential energy of the beam element

The gravitational potential energy of the beam element is taken into account as

$$V_g = \rho A \int_0^l g \cdot (r_0 + r_e) dx \tag{30}$$

where g is the gravitational acceleration vector, and r_o is the vector from the global reference frame to the left-end point of the beam element.

Substituting Eqs. (17) and (18) into (30) leads to

$$V_g = \boldsymbol{G}_e^T \boldsymbol{\delta}_e + D_e \tag{31}$$

where

$$\boldsymbol{G}_e = \rho A \int_0^l (g_x \boldsymbol{N}_u + g_y \boldsymbol{N}_v + g_z \boldsymbol{N}_w) dx \tag{32}$$

$$D_e = \rho A \left[g_x \left(r_{ox} l + \frac{1}{2} l^2 \right) + g_y r_{oy} l + g_z r_{oz} l \right]. \tag{33}$$

3.4. Work done by a tensile load of the beam element

The work done by a tensile load undergoing transverse deflections is given by

$$W_t = \frac{1}{2} \int_0^l P(x,t) \left[\left(\frac{\partial v}{\partial x} \right)^2 + \left(\frac{\partial w}{\partial x} \right)^2 \right] dx \tag{34}$$

where $P(x, t)$ is an axial inertial force, which can be expressed as [28]

$$P(x,t) = P_r - \rho A l \left[a_{ox} + g_x - \frac{1}{2} \left(\omega_{oy}^2 + \omega_{oz}^2 \right) l \right] + \rho A x \left[a_{ox} + g_x - \frac{1}{2} \left(\omega_{oy}^2 + \omega_{oz}^2 \right) x \right] \tag{35}$$

where P_r is an axial load at the right-end point of the beam element, g_x is the x-axis component of the gravitational acceleration.

Substituting Eqs. (17), (18) and (35) into (34) leads to

$$W_t = \frac{1}{2} \boldsymbol{\delta}_e^T \left[\left(\frac{P_r}{l} - \rho A \left(a_{ox} + g_x - \frac{1}{2} (\omega_{oy}^2 + \omega_{oz}^2) l \right) \right) \mathbf{A}_s + \rho A (a_{ox} + g_x) \mathbf{B}_s - \frac{1}{2} \rho A l (\omega_{oy}^2 + \omega_{oz}^2) \mathbf{C}_s \right] \boldsymbol{\delta}_e \tag{36}$$

where

$$\mathbf{A}_s = l \int_0^l \boldsymbol{N}_{vx} \boldsymbol{N}_{vx}^T + \boldsymbol{N}_{wx} \boldsymbol{N}_{wx}^T dx, \qquad \mathbf{B}_s = l \int_0^l x (\boldsymbol{N}_{vx} \boldsymbol{N}_{vx}^T + \boldsymbol{N}_{wx} \boldsymbol{N}_{wx}^T) dx,$$

$$\mathbf{C}_s = \frac{1}{l} \int_0^l x^2 (\boldsymbol{N}_{vx} \boldsymbol{N}_{vx}^T + \boldsymbol{N}_{wx} \boldsymbol{N}_{wx}^T) dx. \tag{37}$$

3.5. Finite element equations

Based on the aforementioned energy and work, the Lagrangian of the beam element can be written as

$$L_e = T_e - V_e - V_g + W_l. \tag{38}$$

Applying the Euler–Lagrange's equation shown in Eq. (9), the finite element equations of the beam element are expressed as

$$\mathbf{M}_e\ddot{\boldsymbol{\delta}}_e + 2\mathbf{B}_e\dot{\boldsymbol{\delta}}_e + (\mathbf{K}_e + \mathbf{K}_d)\boldsymbol{\delta}_e = \boldsymbol{P}_e \tag{39}$$

where

$$\mathbf{K}_d = \dot{\mathbf{B}}_e - \mathbf{M}_s + P_r\mathbf{A}_s + \rho A(a_{ox} + g_x)(-\mathbf{A}_s + \mathbf{B}_s) + \frac{1}{2}\rho Al(\omega_{oy}^2 + \omega_{oz}^2)(\mathbf{A}_s - \mathbf{C}_s) \tag{40}$$

$$\boldsymbol{P}_e = \boldsymbol{G}_e + \boldsymbol{Y}_e - \dot{\boldsymbol{Z}}_e. \tag{41}$$

To assemble all elements, a set of global variables should be defined, which are used to describe the elastic motion of the robot, and they will be introduced in the following section. Besides, the relationship between the global variables and the nodal variables can be expressed as

$$\boldsymbol{\delta}_e = \mathbf{S}_i\boldsymbol{\delta} \tag{42}$$

where $\boldsymbol{\delta}$ is a column vector consisting of the global variables, and $\mathbf{S}_i$ is the transformation matrix from the global variables to the nodal variables for the ith beam element.

To assemble all the beam elements, substituting Eq. (42) into (41) leads to a set of global equations for the robot as

$$\mathbf{M}\ddot{\boldsymbol{\delta}} + \mathbf{C}\dot{\boldsymbol{\delta}} + \mathbf{K}\boldsymbol{\delta} = \boldsymbol{F} \tag{43}$$

where $\mathbf{M}$, $\mathbf{C}$ and $\mathbf{K}$ are the mass matrix, the equivalent damping matrix, and the equivalent stiffness matrix, respectively; and $\boldsymbol{F}$ is the equivalent force vector. The matrices and the vector can be written as

$$\begin{aligned}
&\mathbf{M} = \sum_i \mathbf{S}_i^T\mathbf{M}_e\mathbf{S}_i, \qquad \mathbf{C} = 2\sum_i \mathbf{S}_i^T(\mathbf{M}_e\dot{\mathbf{S}}_i + \mathbf{B}_e\mathbf{S}_i),\\
&\mathbf{K} = \sum_i \mathbf{S}_i^T(\mathbf{M}_e\ddot{\mathbf{S}}_i + 2\mathbf{B}_e\dot{\mathbf{S}}_i + (\mathbf{K}_e + \mathbf{K}_d)\mathbf{S}_i), \qquad \boldsymbol{F} = \sum_i \mathbf{S}_i^T\boldsymbol{P}_e.
\end{aligned} \tag{44}$$

Note that the terms associated with the kinetic energy and the gravitational potential energy of the end-effector should be added into Eq. (43). Besides, a proportional damping matrix ($\mathbf{C}_p = \alpha\mathbf{M} + \beta\mathbf{K}$, where α and β are two coefficients determined by the natural frequencies) can be used as a physical damping, which can be added into the equivalent damping matrix. The major advantage of the proposed model is that it is a set of linear time-varying differential equations, which can be easily solved by most of numerical integrations. Thus, the time responses of the global variables can be determined, so the flexible motion can be obtained.

4. Global variables and transformation matrix

One assumes that the variations of the position and the attitude of the end-effector come from the effects of flexible links. For the position variations, the first three global variables (δ_1, δ_2, δ_3) are defined as the displacement variations of point P. For the attitude variations, another three global variables (δ_4, δ_5, δ_6) are defined as the Euler angles, and they are assumed to be small. Thus, the D–H transformation matrix can be used to express the coordinate transformation from the rigid configuration to the flexible configuration as

$$\mathbf{H}_P = \begin{bmatrix} 1 & -\delta_6 & \delta_5 & \delta_1 \\ \delta_6 & 1 & -\delta_4 & \delta_2 \\ -\delta_5 & \delta_4 & 1 & \delta_3 \\ 0 & 0 & 0 & 1 \end{bmatrix}. \tag{45}$$

To determine the relationship between these six global variables and the flexible links, one considers that point B_i on the upper link has the variations of position and attitude due to the link flexibility, so the variations can be denoted by six nodal variables. Similarly, point D_i on the lower link also has the variations of position and attitude due to the flexibility, so the variations can be denoted by another six global variables. One assumes that the Euler angles are small, so the D–H transformations of points B_i and D_i from the rigid configuration to the flexible configuration can be written as

$$\mathbf{H}_B = \begin{bmatrix} 1 & -\gamma_{B3} & \gamma_{B2} & u_B \\ \gamma_{B3} & 1 & -\gamma_{B1} & v_B \\ -\gamma_{B2} & \gamma_{B1} & 1 & w_B \\ 0 & 0 & 0 & 1 \end{bmatrix}, \qquad \mathbf{H}_D = \begin{bmatrix} 1 & -\gamma_{D3} & \gamma_{D2} & u_D \\ \gamma_{D3} & 1 & -\gamma_{D1} & v_D \\ -\gamma_{D2} & \gamma_{D1} & 1 & w_D \\ 0 & 0 & 0 & 1 \end{bmatrix} \tag{46}$$

where (u_B, v_B, w_B) and (u_D, v_D, w_D) are the variations of the displacement; (γ_{B1}, γ_{B2}, γ_{B3}) and (γ_{D1}, γ_{D2}, γ_{D3}) are the variations of the Euler angles.

Based on the aforementioned descriptions, the D–H transformation matrix can be used to determine the relationship between the global variables of the end-effector and the nodal variables of the flexible links as

$$\mathbf{R}_z(\theta_i)\mathbf{T}_x(r_A)\mathbf{R}_y(\phi_{1i})\mathbf{T}_x(L_1)\mathbf{H}_B P_y(\phi_{2i})\mathbf{R}_z(\phi_{3i})\mathbf{T}_x(L_2)\mathbf{H}_D\mathbf{R}_z(-\phi_{3i})\mathbf{R}_y(-\phi_{i2})\mathbf{T}_x(-r_B) = \mathbf{H}_P \tag{47}$$

where $\mathbf{R}$ and $\mathbf{T}$ are the rotation matrix and the translation matrix, respectively, which are defined in Eq. (2).

Eq. (47) can be expanded, and then the nonlinear terms related to the variation variables, u_B, v_B, w_B, u_D, v_D, w_D, γ_{B1}, γ_{B2}, γ_{B3}, γ_{D1}, γ_{D2}, and γ_{D3}, are eliminated, because they are assumed to be small. Thus, three position equations and three attitude equations can be arranged as

$$\mathbf{M}_B\boldsymbol{V}_B + \mathbf{M}_D\boldsymbol{V}_D = \boldsymbol{V}_P \tag{48}$$

where

$$\boldsymbol{V}_B = [u_B \quad v_B \quad w_B \quad \gamma_{B1} \quad \gamma_{B2} \quad \gamma_{B3}]^T \tag{49}$$

$$\boldsymbol{V}_D = [u_D \quad v_D \quad w_D \quad \gamma_{D1} \quad \gamma_{D2} \quad \gamma_{D3}]^T \tag{50}$$

$$\boldsymbol{V}_P = [\delta_1 \quad \delta_2 \quad \delta_3 \quad \delta_4 \quad \delta_5 \quad \delta_6]^T \tag{51}$$

$$\mathbf{M}_B = \begin{bmatrix} -s_3s_\theta + c_{12}c_3c_\theta & -c_3s_\theta - c_{12}s_3c_\theta & s_{12}c_\theta & r_Bs_{12}c_3s_\theta & r_Bs_{12}s_3s_\theta & r_Bc_{12}s_\theta \\ s_3c_\theta + c_{12}c_3s_\theta & c_3c_\theta - c_{12}s_3s_\theta & s_{12}s_\theta & r_Bs_{12}c_3c_\theta & -r_Bs_{12}s_3c_\theta & -r_Bc_{12}c_\theta \\ -s_{12}c_3 & s_{12}s_3 & c_{12} & r_Bs_3 & r_Bc_3 & 0 \\ 0 & 0 & 0 & -s_3s_\theta + c_{12}c_3c_\theta & -c_3s_\theta - c_{12}s_3c_\theta & s_{12}c_\theta \\ 0 & 0 & 0 & s_3c_\theta + c_{12}c_3s_\theta & c_3c_\theta - c_{12}s_3s_\theta & s_{12}s_\theta \\ 0 & 0 & 0 & -s_{12}c_3 & s_{12}s_3 & c_{12} \end{bmatrix} \tag{52}$$

$$\mathbf{M}_D = \begin{bmatrix} c_1c_\theta & -s_\theta & s_1c_\theta & -r_Bs_1s_\theta + L_2(s_1s_3c_\theta - s_2c_3s_\theta) & -L_2s_{12}c_3c_\theta & r_Bc_1s_\theta - L_2(c_1s_3c_\theta + c_2c_3s_\theta) \\ c_1s_\theta & c_\theta & s_1s_\theta & r_Bs_1c_\theta + L_2(s_2c_3c_\theta + s_1s_3s_\theta) & -L_2s_{12}c_3s_\theta & -r_Bc_1c_\theta + L_2(c_2c_3c_\theta - c_1s_3s_\theta) \\ -s_1 & 0 & c_1 & L_2c_1s_3 & r_B - L_2c_{12}c_3 & L_1s_1s_3 \\ 0 & 0 & 0 & c_1c_\theta & -s_\theta & s_1c_\theta \\ 0 & 0 & 0 & c_1s_\theta & c_\theta & s_1s_\theta \\ 0 & 0 & 0 & -s_1 & 0 & c_1 \end{bmatrix} \tag{53}$$

where c and s represent cosine and sine functions, and the subscripts 1, 2, 3, and θ refer to the function value ϕ_{1i}, ϕ_{2i}, ϕ_{3i}, and θ_i, respectively. The subscript 12 refers to $(\phi_{1i} + \phi_{2i})$.

Eq. (48) represents six equations in terms of twelve nodal variables and six global variables. One intends to convert the equation as a function of the global variables, so the nodal variables shown in Eq. (49) are defined as another six global variables:

$$\boldsymbol{V}_B = [u_B \quad v_B \quad w_B \quad \gamma_{B1} \quad \gamma_{B2} \quad \gamma_{B3}]^T = [\delta_7 \quad \delta_8 \quad \delta_9 \quad \delta_{10} \quad \delta_{11} \quad \delta_{12}]^T. \tag{54}$$

Therefore, the nodal variables in Eq. (48) can be rewritten as

$$\boldsymbol{V}_D = \mathbf{M}_D^{-1}\boldsymbol{V}_P - \mathbf{M}_D^{-1}\mathbf{M}_B\boldsymbol{V}_B. \tag{55}$$

Note that $\boldsymbol{V}_D$ is a function of the twelve global variables, because $\boldsymbol{V}_P$ and $\boldsymbol{V}_B$ refer to the first six and last six global variables, respectively.

To illustrate the transformation matrix $\mathbf{S}_i$ shown in Eq. (42), one considers that each link is discretized with one two-node element, where each node locates at each end of the beam element. Linear functions are used to approximate the axial displacement and the torsional angle of the beam element, and cubic polynomials are used to approximate the two-directional transverse displacements of the beam element. Thus, the beam element has twelve nodal variables, which are given as

$$\boldsymbol{\delta}_e = [u_1 \quad u_2 \quad \varphi_1 \quad \varphi_2 \quad v_1 \quad v_2 \quad v_3 \quad v_4 \quad w_1 \quad w_2 \quad w_3 \quad w_4]^T \tag{56}$$

where u_1 and u_2 are the axial displacements at both nodes of the beam element; φ_1 and φ_2 are the torsional angles at both nodes; v_1 and v_3 are the y-axis transverse displacements at both nodes; v_2 and v_4 are the first derivatives of the y-axis transverse displacements; w_1 and w_3 are the z-axis transverse displacements at both nodes; v_2 and v_4 are the first derivatives of the z-axis transverse displacements.

By applying adequate boundary conditions, all nodal variables can be expressed as functions of the global variables.

For the upper link, the nodal variables at point A_i and B_i are respectively written as

$$u_1 = \varphi_1 = v_1 = v_2 = w_1 = w_2 = 0 \tag{57}$$

$$[u_2 \quad \varphi_2 \quad v_3 \quad v_4 \quad w_3 \quad w_4] = [\delta_7 \quad \delta_{10} \quad \delta_8 \quad \delta_{11} \quad \delta_9 \quad \delta_{12}]. \tag{58}$$

Table 1
Parameters of the manipulator.

Parameter	Symbol	Value	Unit
Length of upper link	L_1	0.5	m
Length of lower link	L_2	0.6	m
Distance from points O to A	r_A	0.1	m
Distance from points P to D	r_B	0.05	m
Thickness of link	h	5×10^{-3}	m
Width of link	w	5×10^{-3}	m
Mass density	ρ	7.8×10^3	kg/m^3
Elastic modulus	E	210	GPa
Shear modulus	G	80	GPa
Mass of end-effector	m_p	0.5	kg
Thickness of end-effector	h_p	0.05	m

For the lower link, the nodal variables at point B_i and D_i are respectively written as

$$\begin{bmatrix} u_1 \\ v_1 \\ w_1 \end{bmatrix} = \begin{bmatrix} c_1 & 0 & -s_1 \\ 0 & 1 & 0 \\ s_1 & 0 & c_1 \end{bmatrix} \begin{bmatrix} \delta_7 \\ \delta_8 \\ \delta_9 \end{bmatrix}, \qquad \begin{bmatrix} \varphi_1 \\ v_2 \\ w_2 \end{bmatrix} = \begin{bmatrix} 0 \\ \delta_{13} \\ \delta_{14} \end{bmatrix} + \frac{1}{L_2} \begin{bmatrix} 0 \\ V_{D2} - v_1 \\ V_{D3} - w_1 \end{bmatrix} \tag{59}$$

$$\begin{bmatrix} u_2 \\ v_3 \\ w_3 \end{bmatrix} = \begin{bmatrix} V_{D1} \\ V_{D2} \\ V_{D3} \end{bmatrix}, \qquad \begin{bmatrix} \varphi_2 \\ v_4 \\ w_4 \end{bmatrix} = \begin{bmatrix} V_{D4} \\ V_{D5} \\ V_{D6} \end{bmatrix} + \frac{1}{L_2} \begin{bmatrix} 0 \\ V_{D2} - v_1 \\ V_{D3} - w_1 \end{bmatrix} \tag{60}$$

where the numbers of the subscripts of V_D refer to the row number; δ_{13} and δ_{14} are two additional global variables associated with the transverse displacements at point B_i; the second terms of the second equations in Eqs. (59) and (60) refer to the angle produced by the displacement variations of points B_i and D_i.

Eqs. (57)–(60) perform the nodal variables as linear functions of the global variables for the two links of each kinematic chain, so the functions can be written as Eq. (42). Thus, the transformation matrix $\mathbf{S}_i$ can be obtained. The aforementioned derivations can be straightforwardly extended to the links discretized as multiple elements, and the total number of degrees of freedom of the manipulator can be given by

$$\text{DOF} = 6 + 3 \times (12n - 4) \tag{61}$$

where n is the number of elements per link, the first term 6 refers to the degrees of freedom of the end-effector, and the bracket in the second term refers to the degrees of freedom of each kinematic chain. Thus, for the one-element discretization per link, the total degrees of freedom are thirty.

5. Numerical simulations

The parameters of the manipulator are listed in Table 1.

5.1. Natural frequency analysis

Since the natural frequencies of the robot depend on its configurations, a circular motion of point P along the Z-axis is considered, where the center and the radius of the circle are (0, 0, 0.5) m and 0.1 m, respectively. Each point on the circle can determine a specific configuration of the robot based on the inverse kinematics. Thus, the natural frequencies can be expressed as functions of the rotating angle along the Z-axis. In this simulation, each link of the robot is modeled by one beam element, and the axial displacement and the torsional angle are approximated by linear polynomials, and the two transverse displacements are approximated by cubic polynomials. Fig. 4 shows the first eight natural frequencies with respect to the rotating angle along the Z-axis. The result shows that each natural frequency varies between certain ranges. Since the points A_i ($i = 1, 2, 3$) form an equilateral triangle from the top view of the robot, the natural frequencies will repeat every 120°, and this property can be shown in Fig. 4.

5.2. Convergence analysis

To show the convergence of the presented model, the configuration of the manipulator is considered with the coordinate of point P at (0.1, 0, 0.5), and each link of the robot is discretized as multiple beam elements. Table 2 shows the first eight natural frequencies for the number of elements per link increasing from one to eight, where the axial displacement and the torsional angle are approximated by linear polynomials, and the two transverse displacements are approximated by cubic polynomials. The results show that the natural frequencies converge as the number of elements increases. Besides, the higher-mode natural frequencies converge with more elements. To obtain faster rates of convergence, the degrees of approximation functions increase. Table 3 also shows that the first eight natural frequencies for the number of elements

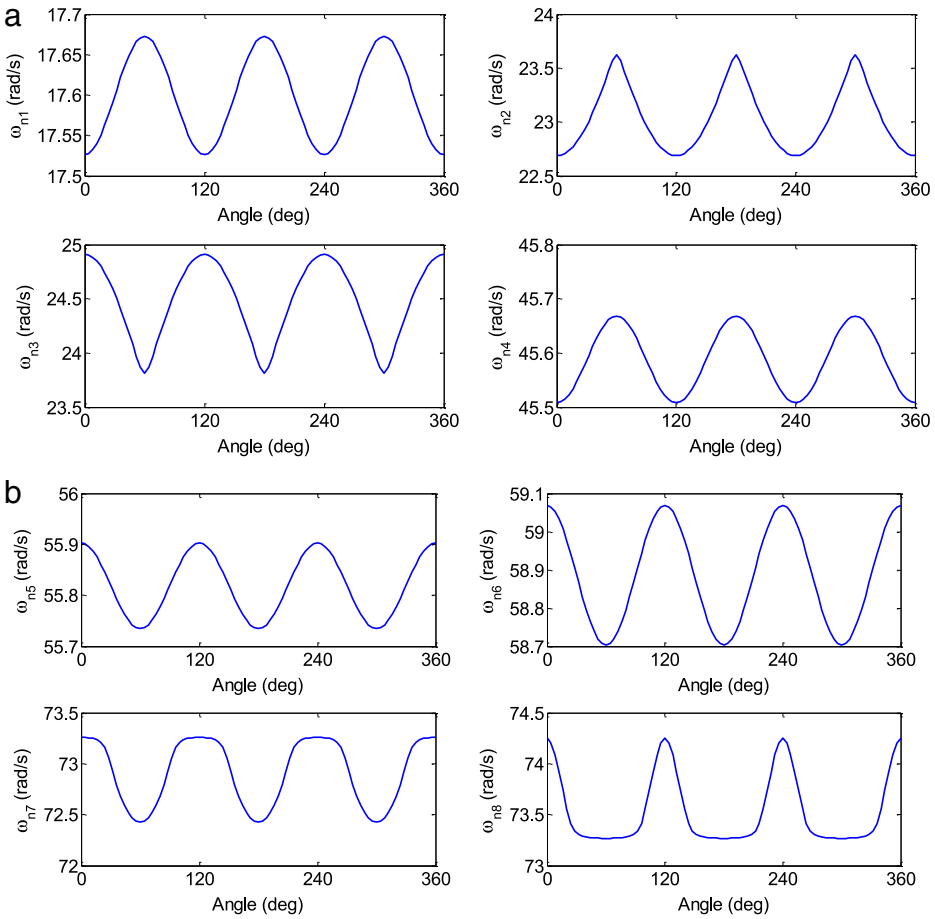

Fig. 4. Natural frequencies as functions of angles, (a) the first to the fourth natural frequencies; (b) the fifth to the eighth natural frequencies.

Table 2
Natural frequencies based on linear and cubic approximations.

n	DOF	Natural frequencies (rad/s)							
		ω_{n1}	ω_{n2}	ω_{n3}	ω_{n4}	ω_{n5}	ω_{n6}	ω_{n7}	ω_{n8}
1	30	17.5268	22.6970	24.9179	45.5980	56.0472	59.3049	73.5428	74.5347
2	66	17.5261	22.6893	24.9091	45.5159	55.9132	59.0846	73.2860	74.2730
3	102	17.5260	22.6889	24.9086	45.5096	55.9047	59.0718	73.2643	74.2530
4	138	17.5260	22.6888	24.9085	45.5084	55.9032	59.0696	73.2604	74.2494
5	174	17.5260	22.6888	24.9085	45.5081	55.9028	59.0690	73.2594	74.2484
6	210	17.5260	22.6888	24.9084	45.5080	55.9027	59.0687	73.2590	74.2481
7	246	17.5260	22.6888	24.9084	45.5079	55.9026	59.0686	73.2588	74.2479
8	282	17.5260	22.6888	24.9084	45.5079	55.9026	59.0686	73.2587	74.2479

n: Number of elements.
DOF: Degrees of freedom.

per link increasing from one to four, where the axial displacement and the torsional angle are approximated by cubic polynomials and the two transverse displacements are approximated by quintic polynomials. The results show that these natural frequencies converge with a two-element discretization.

5.3. Steady state response analysis

To obtain a steady state response, the end-effector is assigned to follow a circular path, whose center and radius are (0, 0, 0.5) and 0.1 m, respectively. Besides, the rotating period is one second, and a five-period numerical integration is performed by the Newmark method with a constant time step. Fig. 5 shows the time responses of the applied torques at the active joints, and the results show that the applied torques are periodic functions of time. Figs. 6 and 7 show the time responses of

Table 3
Natural frequencies based on cubic and quintic approximations.

n	DOF	Natural frequencies (rad/s)							
		ω_{n1}	ω_{n2}	ω_{n3}	ω_{n4}	ω_{n5}	ω_{n6}	ω_{n7}	ω_{n8}
1	78	17.5260	22.6888	24.9084	45.5079	55.9025	59.0685	73.2586	74.2478
2	138	17.5260	22.6888	24.9084	45.5079	55.9025	59.0685	73.2586	74.2477
3	198	17.5260	22.6888	24.9084	45.5079	55.9025	59.0685	73.2586	74.2477
4	258	17.5260	22.6888	24.9084	45.5079	55.9025	59.0685	73.2586	74.2477

n: Number of elements.
DOF: Degrees of freedom.

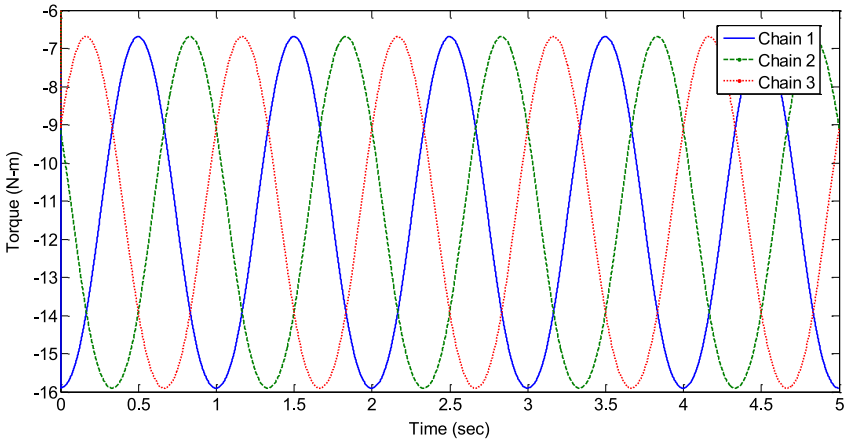

Fig. 5. Time responses of the applied torques on the active joints.

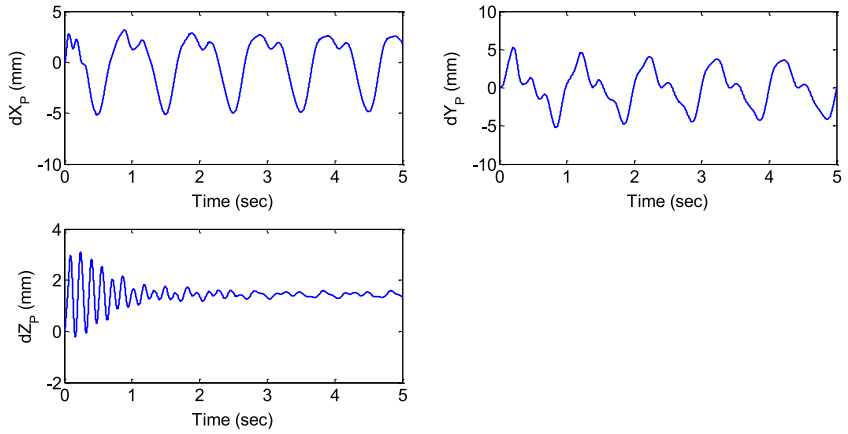

Fig. 6. Time responses of the position variations of the end-effector due to the link flexibility.

the position and attitude variations of the end-effector due to the flexibility of links. Since the gravitational effect is taken into account, there is a small variation along the positive z-axial direction. Fig. 8 shows the time responses of the axial displacements of the links at the half-length locations, and the results show that there are small displacements of the upper links to compare with those of the lower links. Fig. 9 shows the time responses of the torsional angles of the links, and the results show that the angles of the upper links are greater than those of the lower links. Fig. 10 shows the time responses of the y-axis transverse displacements, and the results show that the displacements of the lower links are greater than those of the upper links. Fig. 11 shows the time responses of the z-axis transverse displacements, and the results show that the strains of the lower links are greater than those of the upper links. Furthermore, Figs. 5 and 8–11 not only indicate that these time responses are the periodic functions of time at the steady state but also show that there are the same phase shifts between the time responses of the three kinematic chains. The reason is that there are the differences 120° of the locations of any two kinematic chains from the top view of the robot.

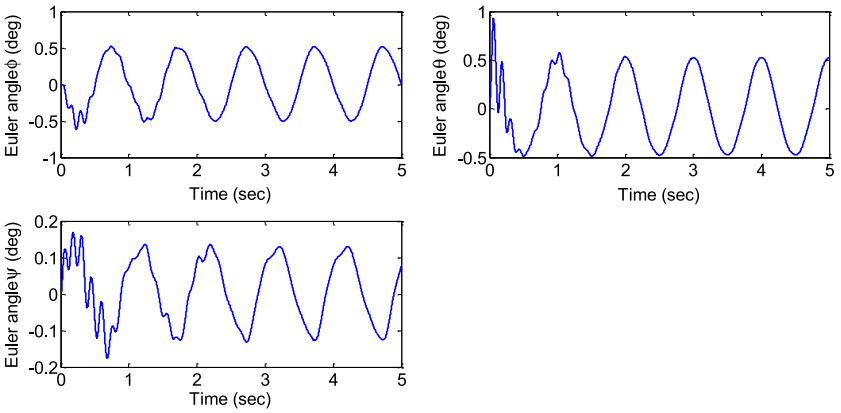

Fig. 7. Time responses of the attitude variations of the end-effector due to the link flexibility.

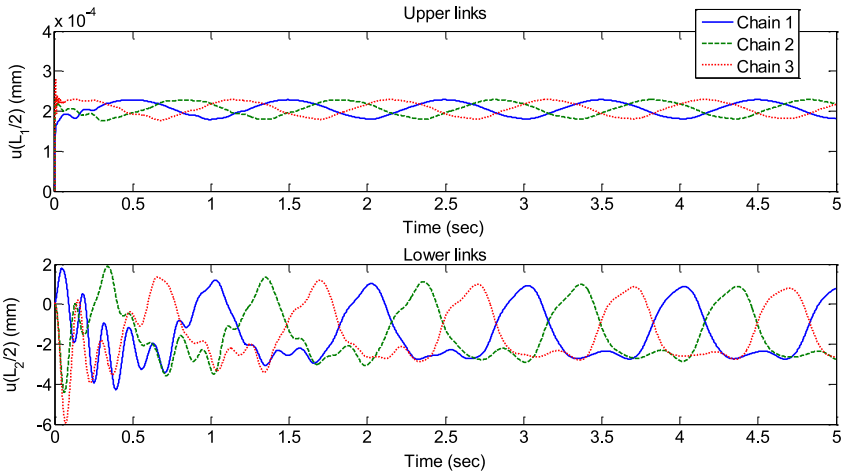

Fig. 8. Time response of the axial displacements of the links at the half-length locations.

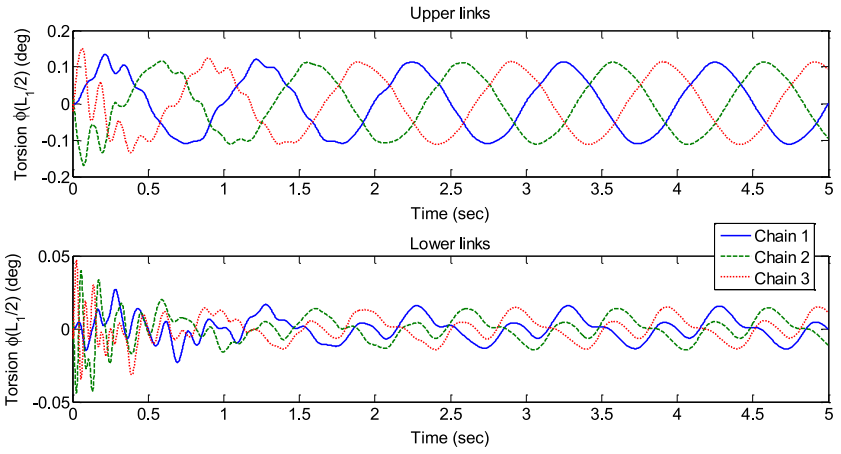

Fig. 9. Time response of the torsional angles of the links at the half-length locations.

5.4. Vibration analysis based on an inverted-U trajectory

The Delta robot is usually applied to machining or assembling based on a desired moving trajectory of the end-effector, and an inverted-U trajectory is one of the commonly used moving paths for a pick-and-place operation in industry. One assumes that the original position of the end-effector is at coordinates (X_0, Y_0, Z_0), and the final position is at $(X_0 + d_X,$

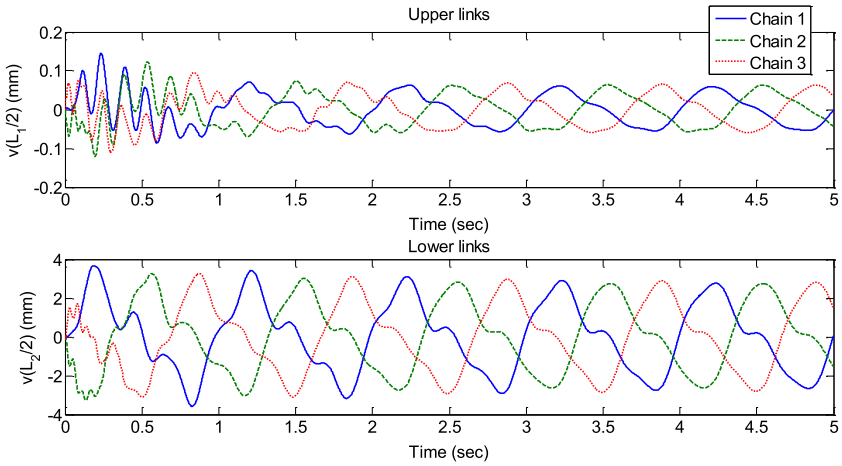

Fig. 10. Time response of the y-axis transverse displacements of the links at the half-length locations.

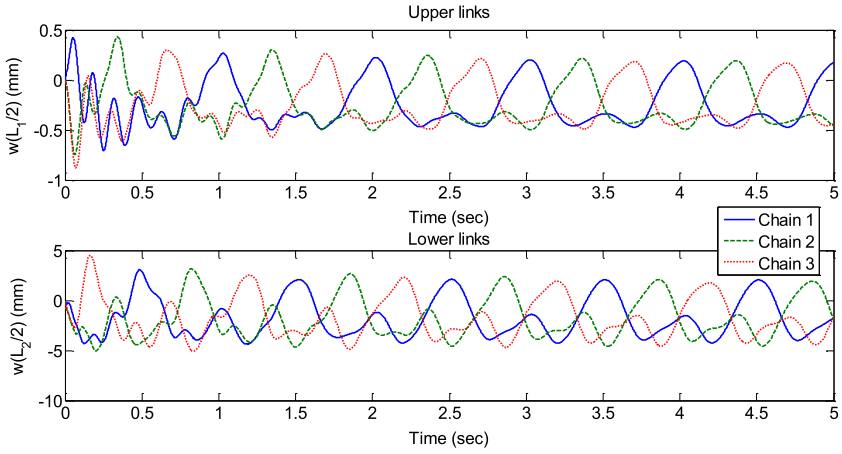

Fig. 11. Time response of the z-axis transverse displacements of the links at the half-length locations.

$Y_0 + d_Y, Z_0$). During the moving process, the end-effector first moves from coordinate Z_0 to $Z_0 + d_Z$ and then moves back to Z_0. Thus, the entire trajectory is an inverted-U path. Besides, the entire motion is executed from time t_0 to t_f, and three additional set points are defined as time t_1, t_2 and t_3 during the moving period. From time t_1 to t_3, the end-effector moves from the positions $(X, Y) = (X_0, Y_0)$ to $(X_0 + d_X, Y_0 + d_Y)$. From time t_0 to t_2, the end-effector moves from $Z = Z_0$ to $Z_0 + d_Z$. From time t_2 to t_f, the end-effector moves back from $Z = Z_0 + d_Z$ to Z_0. In order to have zero velocities, accelerations and jerks at each step point, a septic polynomial is applied to each moving interval.

One sets the time $(t_0, t_1, t_2, t_3, t_f)$, an initial position, and a moving distance (d_X, d_Y, d_Z) as (0, 0.2, 0.4, 0.6, 0.8) s, (−0.08, −0.02, 0.5) m, and (0.16, 0.04, 0.2) m, respectively. Fig. 12 shows the moving trajectory of the end-effector represented as position, velocity and acceleration functions of time, and the figure shows that the functions are smooth in time. Fig. 13 shows the desired moving path represented in coordinates (X, Y, Z), and the figure shows an inverted-U path. Fig. 14 shows the time responses of the applied torques on the active joints, and the result shows that torque functions are smooth in time. Fig. 15 shows the time responses of the position variations of the end-effector. The results show that the maximum position variations are (−13.05, 3.520, −8.691) mm, and the final position variations are (−1.228, −0.1862, 1.197) mm. Fig. 16 shows the time responses of the attitude variations of the end-effector. The results show that the maximum attitude variations are (0.1479, 0.5075, 0.01672) degrees, and the final attitude variations are $(6.473 \times 10^{-2}, 4.491 \times 10^{-1}, 8.246 \times 10^{-3})$ degrees.

6. Conclusions

This paper presents a modeling of a Delta robot with flexible links. The model is based on the kinematics of the rigid body motions of the robot, and the flexibilities of the links are superimposed in the rigid body motions. To model the flexibility, the finite element method is applied to establish a beam element with translating and rotating motions on a floating reference frame, where the deformations of the links are assumed to be small. The model of the robot is derived by using the Euler–Lagrange's equation without using any constraint equations, so the number of equations is not increased. To

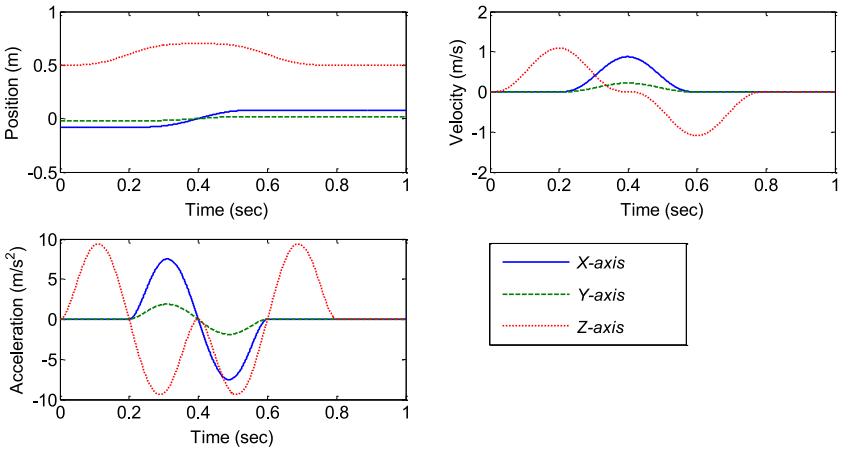

Fig. 12. Desired trajectory of the end-effector.

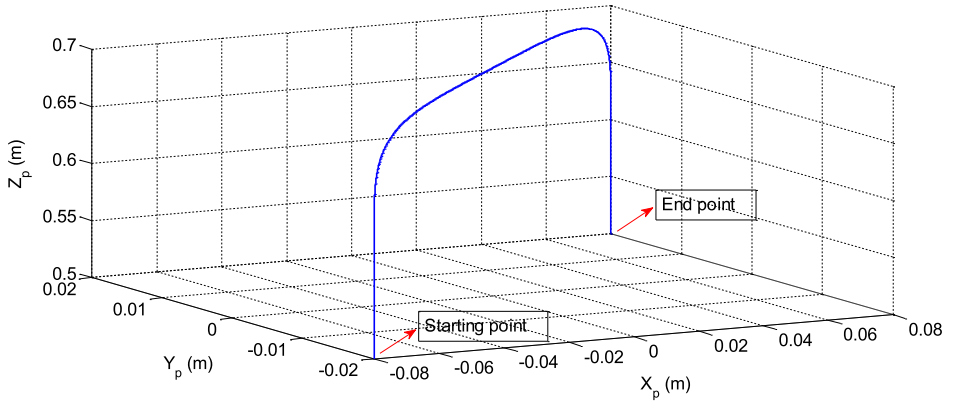

Fig. 13. Desired moving path of the end-effector.

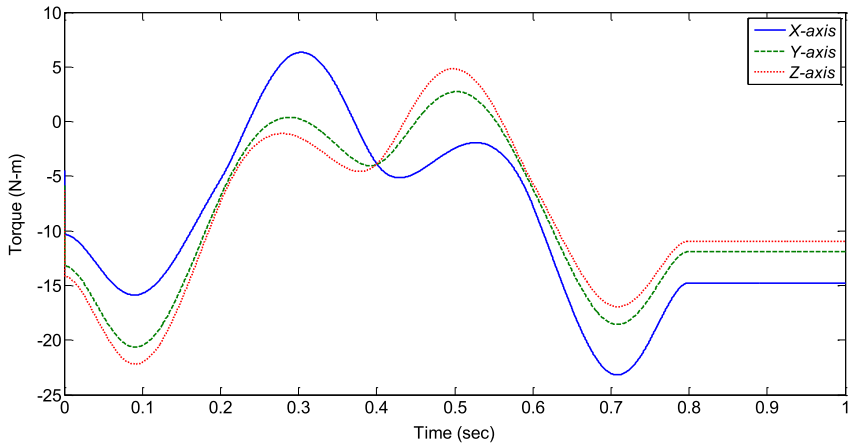

Fig. 14. Time responses of the applied torques on the active joints.

assemble all elements, one applies the D–H method to determine the relationship between the global variables and the nodal variables, which can be expressed as a set of linear algebraic equations. After assembling all elements, the finite element equations of the robot are a set of linear time-varying differential equations, so they can be easily solved by numerical integrations.

Based on the proposed model, there are four numerical simulations presented. First, the natural frequency analysis is performed based on a circular motion. The results show that each natural frequency varies in a certain range has a

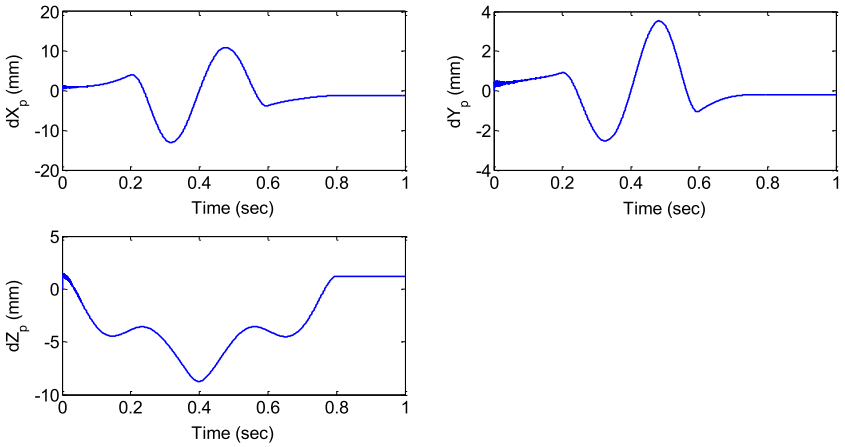

Fig. 15. Time responses of the position variations of the end-effector.

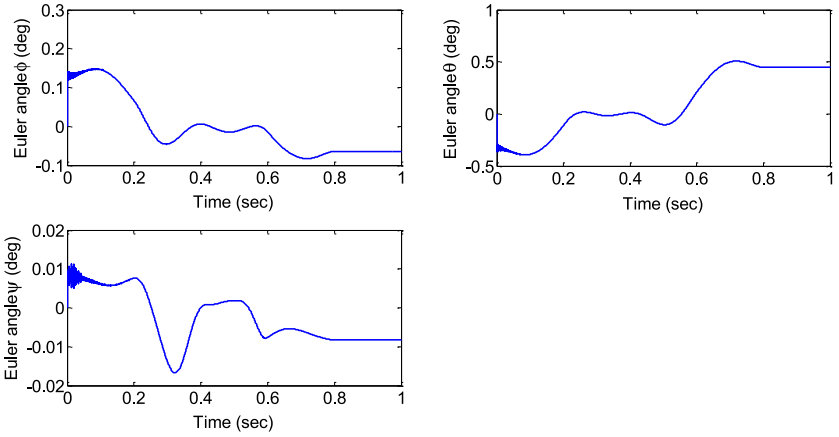

Fig. 16. Time responses of the attitude variations of the end-effector.

period of 120°. Secondly, the convergence analysis is presented. The results show that the approximation with a higher degree of polynomials has a higher convergence rate and a smaller number of degrees of freedom, which implies the less computational time. Thirdly, a numerical simulation based on a circular motion is demonstrated. The results show that the end-effector has the variations, which are approximately ± 5 mm on the X–Y plane, 1.5 mm along the Z-axis, $\pm 0.5°$ along the X- and Y-axes, and $\pm 0.15°$ along the Z-axis. Finally, another numerical simulation based on an inverted-U path to simulate an industrial pick-to-place motion is demonstrated. The results show that the maximum variations are around 10 mm and 5° due to the flexibilities of links. Thus, for the robot required to operate with a high positioning accuracy, the path planning of the robot should include the effect of the flexibility. Since the proposed model considers only the flexibility of links, and all joints are assumed to be ideally fixed and revolute, these assumptions should be relaxed so as to have a more accurate mathematical model. Furthermore, an experimental setup and validation may be performed to be a modification reference for the mathematical model.

Acknowledgment

The study was sponsored with a research grant, MOST-102-2221-E-011-073, from the Ministry of Science and Technology, Taiwan.

References

[1] R. Clavel, DELTA, a fast robot with parallel geometry, in: International Symposium on Industrial Robots, 1988, pp. 91–100.
[2] P. Vischer, R. Clavel, Kinematic calibration of the parallel delta robot, Robotica 16 (2) (1998) 207–218.
[3] F. Pierrot, C. Reynaud, A. Fournier, DELTA: A simple and efficient parallel robot, Robotica 8 (2) (1990) 105–109.
[4] C.R. Boër, L. Molinari-Tosatti, K.S. Smith (Eds.), Parallel Kinematic Machines: Theoretical Aspects and Industrial Requirements, Springer, 2011.
[5] C. Gosselin, Kinematic analysis, optimization and programming of parallel robotic manipulators (Ph.D. Thesis), University of McGill, 1988.
[6] L.W. Tsai, Robot Analysis: The Mechanics of Serial and Parallel Manipulator, Wiley, Wiley, 1999.

[7] M.A. Laribi, L. Romdhane, S. Zeghloul, Analysis and dimensional synthesis of the DELTA robot for a prescribed workspace, Mech. Mach. Theory 42 (2007) 859–870.
[8] K. Miller, Experimental verification of modeling of DELTA robot dynamics by direct application of Hamilton's principle, in: IEEE International Conference on Robotics and Automation, vol. 1, 1995, pp. 532–537.
[9] J. Li, J. Wang, W. Chou, Y. Zhang, T. Wang, Q. Zhang, Inverse kinematics and dynamics of the 3-RRS parallel platform, in: IEEE International Conference on Robotics and Automation, vol. 3, 2001, pp. 2506–2511.
[10] S. Staicu, D.C. Carp-Ciocardia, Dynamic analysis of Clavel's delta parallel robot, in: IEEE International Conference on Robotics and Automation, vol. 3, 2003, pp. 4116–4121.
[11] K.S. Hsu, M. Karkoub, M.C. Tsai, M.G. Her, Modelling and index analysis of a delta-type mechanism, Proc. Inst. Mech. Eng. Part K J. Multi-body Dyn. 218 (3) (2004) 121–132.
[12] S.B. Park, H.S. Kim, C. Song, K. Kim, Dynamics modeling of a delta-type parallel robot, in: The 44th International Symposium on Robotics, 2013, pp. 1–5.
[13] W.J. Book, Recursive Lagrangian dynamics of flexible manipulator arms, Int. J. Robot. Res. 3 (3) (1984) 87–101.
[14] M. Géradin, A. Cardona, Flexible Multibody Dynamics: A Finite Element Approach, Wiley, 2001.
[15] A. Fattah, J. Angeles, A.K. Misra, Dynamics of a 3-DOF spatial parallel manipulator with flexible links, in: IEEE International Conference on Robotics and Automation, vol. 1, 1995, pp. 627–633.
[16] S. Liu, Z. Zhu, B. Zi, C. Liu, Y. Yu, Dynamics of 3-DOF spatial parallel manipulator with flexible links, in: International Conference on Mechanic Automation and Control Engineering, 2010, pp. 2327–2331.
[17] M. Rognant, E. Courteille, P. Maurine, A systematic procedure for the elastodynamic modeling and identification of robot manipulators, IEEE Trans. Robot. 26 (6) (2010) 1085–1093.
[18] L. Zhang, Y. Song, Optimal design of the delta robot based on dynamics, in: IEEE International Conference on Robotics and Automation, 2011, pp. 336–341.
[19] L. Březina, M. Holub, L. Cintula, J. Kovar, Delta robot design, Solid State Phenom. 198 (2013) 9–14.
[20] W.L. Cleghorn, R.G. Fenton, B. Tabarrok, Finite element analysis of high-speed flexible mechanisms, Mech. Mach. Theory 16 (4) (1981) 407–424.
[21] W.L. Cleghorn, R.G. Fenton, B. Tabarrok, Steady-state vibrational response of high-speed flexible mechanisms, Mech. Mach. Theory 19 (4–5) (1984) 417–423.
[22] G. Piras, W.L. Cleghorn, J.K. Mills, Dynamic finite-element analysis of a planar high-speed, high-precision parallel manipulator with flexible links, Mech. Mach. Theory 40 (7) (2005) 849–862.
[23] P.E. Gaultier, W.L. Cleghorn, A spatially translating and rotating beam finite element for modeling flexible manipulators, Mech. Mach. Theory 27 (4) (1992) 415–433.
[24] M. Grubler, Getriebelehre, Springer, 1917.
[25] K. Kutzbach, Mechanische Leitungsverzweigung, Maschinenbau, Der Betreib 8 (21) (1929) 710–716.
[26] J. Denavit, R.S. Hartenberg, A kinematic notation for lower-pair mechanisms based on matrices, Trans. ASME J. Appl. Mech. 23 (1955) 215–221.
[27] A.A. Shabana, Dynamics of Multibody Systems, Cambridge, 2013.
[28] L. Meirovitch, Fundamentals of Vibrations, McGraw-Hill, 2002.